Geophysical Journal International

Geophys. J. Int. (2024) **236,** 431–442
Advance Access publication 2023 November 09
GJI Geomagnetism and Electromagnetism

https://doi.org/10.1093/gji/ggad423

Palaeomagnetic field intensity measurements from the 2.6 Ga Yandinilling dyke swarm (Western Australia)

Louise M. Hawkins,[1] Andrew J. Biggin,[1] Yebo Liu,[2] J. Michael Grappone[1] and Zheng-Xiang Li[2]

[1]*Geomagnetism Laboratory, Department of Earth, Ocean and Ecological Sciences, University of Liverpool, Liverpool L697ZE, UK. E-mail: A.Biggin@liverpool.ac.uk*
[2]*Earth Dynamics Research Group, The Institute for Geoscience Research (TIGeR), School of Earth and Planetary Sciences, Curtin University, Bentley, WA 6102, Australia*

Accepted 2033 October 31. Received 2023 October 12; in original form 2022 October 31

SUMMARY

Precambrian palaeointensity measurements provide fundamental constraints on the evolution of the deep Earth. Core evolution models predict trends in dipole moment on billion-year timescales that can be tested by palaeomagnetic records. Here, we report new palaeointensity results from the recently identified ∼2.62 Ga Yandinilling dyke swarm of the Yilgarn Craton, Western Australia, and consider them alongside published measurements spanning 500 Myr across the late Archaean to earliest Proterozoic. Rock magnetic and scanning electron microscopy analysis confirm that the magnetic mineralogy is fine-grained magnetite, appearing mostly as exsolved lamellae with ilmenite. Six sites produced acceptable palaeointensity estimates from thermal and microwave IZZI protocol Thellier experiments and from double-heating technique Shaw experiments. These site mean values of 9–26 μT translate to virtual dipole moments of 11–44 ZAm^2 that are considerably lower than today's dipole moment of ∼80 ZAm^2 and the value predicted for this time period by some thermal evolution models. Their average (median = 41 ZAm^2) is, however, similar to the long-term average during both of the intervals 2300–2800 Ma (median = 44 ZAm^2; $N = 103$) and 10–500 Ma (median 41 ZAm^2; $N = 997$). While there is little evidence for a substantial net change in average dipole moment between the late Archaean and Phanerozoic, there is preliminary evidence that its variance has increased between the two intervals. This lower variance more than two billion years ago supports the idea that the geodynamo, even while not producing a stronger magnetic field, was more stable on average at the Archaean–Proterozoic transition than it is today.

Key words: Australia; Magnetic field variations through time; Palaeointensity; Palaeomagnetism.

INTRODUCTION

The Earth is known to have had a geomagnetic field since at least 3.45 Ga (Biggin *et al.* 2011). The present-day geodynamo is driven largely by thermochemical convection due to the release of light elements at the inner-core boundary (Braginsky 1963). Prior to inner core nucleation (ICN), secular cooling was likely to be the primary control on the geodynamo (Landeau *et al.* 2017), although other mechanisms such as the exsolution of light elements (Badro *et al.* 2016; O'Rourke & Stevenson 2016; Mittal *et al.* 2020) and tidal deformation (Le Bars *et al.* 2011; Landeau *et al.* 2022) may also have been involved. Estimates for the onset of ICN range from 2.5 Ga (Buffett *et al.* 1996) to <500 Ma (Davies *et al.* 2015; Labrosse 2015), based on different thermal properties and associated histories of the core of the Earth. Palaeomagnetism, and the absolute palaeointensity record specifically, have been proposed as a means to estimate when ICN occurred. The dipole moment may have decreased with time prior to ICN because, as the Earth cooled, less energy was available to drive thermal convection. A sharp increase in field strength is predicted at ICN as thermochemical convection became the dominant process (Aubert *et al.* 2009; Davies *et al.* 2022).

Various perceived trends in the Precambrian dipole moment have been interpreted in terms of signatures of stages in Earth's core evolution. Biggin *et al.* (2015) proposed that ICN occurred between 1.5 and 1.0 Ga based on palaeointensities that were higher than in the preceding billion year interval. However, this interpretation was questioned (Smirnov *et al.* 2016), and new evidence suggested that the original study of the 1.3 Ga Gardar lavas on which this conclusion was partly based, was unreliable (Kodama *et al.* 2019).

Notwithstanding the serious doubts over the Gardar lavas, studies from the mid-continent rift (MCR) have confirmed that the field was strong at 1.1 Ga, with intensities similar to the mean palaeofield strength for the last 10–15 Myr (Sprain *et al.* 2018; Zhang *et al.* 2022), which could still represent an increase in the strength of the field after ICN.

A glut of recent palaeointensity studies have also shown that the geomagnetic field was especially weak in the late Ediacaran period (550–600 Ma, Bono *et al.* 2019; Shcherbakova *et al.* 2019; Thallner *et al.* 2021a,b, 2022). These new data have been argued to signify the period immediately before ICN (Bono *et al.* 2019; Zhou *et al.* 2022), although the weak field interval may have continued into the early Cambrian at least (Lloyd *et al.* 2022).

It is difficult to discriminate between different interpretations of the timing of ICN because of the low temporal density of Precambrian dipole moment data. The lack of dipole moment data makes determining the average strength and expected variation of the Precambrian field difficult. Without this understanding, it is difficult to reliably identify deviations in Precambrian field strength that might represent ICN. Further complications arise from the issue that field strength observations observed in the Phanerozoic, such as geomagnetic secular variation (on timescales of <1 Myr) and longer-term variations in dipole moment on timescales of 10–100 Myr, may be misinterpreted as deviations in field strength due to the evolution of the core. Variations on timescales of 10–100 Myr, likely a consequence of mantle convection causing variations in core–mantle heat flux (Biggin *et al.* 2012), have been observed in the mid-Neoproterozoic and late Mesoproterozoic (Lloyd *et al.* 2021). There are also other processes that could affect the strength of the Precambrian field and potentially be misinterpreted as the signal of ICN. These include the precipitation of multiple light elements in the core (Mittal *et al.* 2020) and a shift in the depth of buoyancy generation within the core (Aubert *et al.* 2009; Landeau *et al.* 2017).

Our understanding of Precambrian palaeomagnetic field strength is hampered by the paucity of the dipole moment measurements for this period. Precambrian rock targets suitable for palaeointensity are difficult to find due to pervasive overprinting occurring alongside issues commonly faced with younger samples such as contamination by non-ideal magnetic carriers. The Archaean Yilgarn Craton, Western Australia has strong potential, however, as it hosts at least six generations of Precambrian dykes, some of which have already produced robust palaeointensity results. The 2.41 Ga Widgiemooltha dyke swarm (WDS, Nemchin & Pidgeon 1997) provided the oldest palaeointensity results published for the Yilgarn Craton (Smirnov *et al.* 2013; Smirnov & Evans 2015) prior to this study and yielded a relatively high field dipole moment (66.5 ZAm^2). Such a result is consistent with the prediction of the thermal evolution model favoured by Bono *et al.* (2019) and Zhou *et al.* (2022), which is associated with ICN at ~550 Ma. This particular thermal evolution model, unlike some others (see e.g. Davies *et al.* 2022), favours a strong dipole moment (~60 ZAm^2) throughout the Archaean as a consequence of vigorous thermal convection occurring in the core.

The recently identified ~2.62 Ga Yandinilling dyke swarm (YDS; Stark *et al.* 2018) is now the oldest identified dyke swarm of the Yilgarn Craton and its age makes it an ideal target to evaluate whether the field was consistently strong during the early Precambrian. This study will present new, reliable palaeointensity estimates from the YDS, synthesize them with published data sets from the late Archaean-earliest Proterozoic, and compare this distribution of dipole moment values with that from the Phanerozoic to gain insight into the net evolution of the palaeomagnetic field.

GEOLOGICAL BACKGROUND

The NE trending, mafic YDS extends for > 150 km within the Southwest Terrane, in the southwestern part of the craton, based on geological mapping and aeromagnetic data (Fig. 1). The Southwest terrane, which is largely comprised of granitic and high-grade supracrustal rocks (Pidgeon & Wilde 1990), is one of the most recent Yilgarn terrane to be amalgamated into the craton. This amalgamation occurred between 2652 and 2625 Ma (Wilde & Pidgeon 1987; Nemchin & Pidgeon 1997; McFarlane 2010) and was accompanied by widespread granitic magmatism (Champion & Sheraton 1997) and gold mineralization (Kent *et al.* 1996). The YDS was emplaced at 2615 ± 6 Ma based on ID-TIMS on baddeleyite and 2610 ± 25 Ma based on *in-situ* SHRIMP U-Pb dating of baddeleyite of site 13/R (Stark *et al.* 2018). The timing of emplacement fits well with magmatism generation being due to the proposed delamination or convective thinning of dense eclogite in the lower lithosphere (Smithies & Champion 1999). Alternately, an upwelling mantle plume could explain the emplacement of the mafic dyke swarm (Stark *et al.* 2018).

PALAEOMAGNETISM

The samples used in this study were collected from unweathered dolerite dykes. Each site represents an individual dyke and the samples come from the same locations as sites of the same name reported by previous dating (Stark *et al.* 2018) and palaeomagnetic (Liu *et al.* 2021) studies (samples donated with an R represent the same site that had been resampled at a later date). Liu *et al.* (2021) measured the palaeomagnetic directions of the YDS, isolating the characteristic remanent magnetization (ChRM) between 530–565 and 570–580 °C. This magnetization is considered to be primary based on a positive reversal test ('C' classification; McFadden & McElhinny 1990) and a suggestive baked contact test (the instability of the magnetization preserved by the baked granite host means that the test was not conclusive). Additional evidence that the sites had not been completely remagnetized comes from (i) the preservation of a partial thermal overprint with directions similar to the younger WDS at some of the sites, and (2) the inconsistency between the ChRM directions and any of the published younger palaeomagnetic directions from the region.

MAGNETIC MINERALOGY

The nature of the magnetic remanence carriers in the samples measured for palaeointensity was determined from a combination of thermomagnetic measurements and scanning electron microscopy (SEM). Magnetic susceptibility versus temperature (κ–T) curves were collected using Agico Kappabridge instruments at both the University of Liverpool and at Curtin University. Temperature-dependent magnetization measurements were collected using the University of Liverpool's Magnetic Measurements Variable Field Translation Balance (MMVFTB). All thermomagnetic measurements were run on crushed specimens in air to highlight the potential for alteration that may affect the samples during the palaeointensity experiments. The specimens were heated up to 600–700 °C and some samples showing irreversible thermomagnetic curves were chosen for cyclic heating experiments (peak temperature increased in 100 °C steps between 200 and 700 °C) to determine the temperature range responsible for the alteration. SEM and energy dispersive X-ray (EDX) analyses were performed on polished thin sections

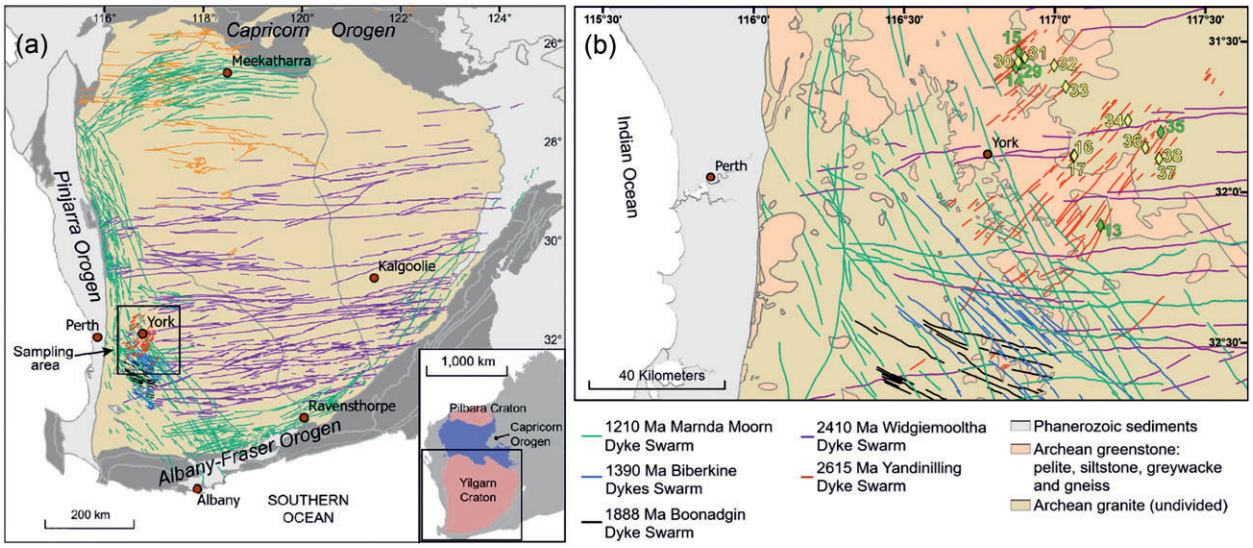

Figure 1. (a) Map of the Yilgarn Craton showing the six known generations of Proterozoic dyke swarms (Stark *et al.* 2018), including the YDS, which is the focus of this study. (b) Map of the sampling area, including all of the sites that have been that were sampled for palaeodirection (Liu *et al.* 2021); yellow diamonds/text) and the sites also used for palaeointensity (green diamonds/text).

prepared from representative core samples from each site that produced palaeointensity results that passed selection criteria used a JEOL JSM-7001F FEGSEM at the Imaging Centre at Liverpool (ICaL).

All the specimens that provided reliable palaeointensity results show sharp drops in magnetic susceptibility at ∼565–580 °C indicating a Curie Temperature (T_C) close to that of pure magnetite (Figs 2a–c). The MMVFTB results are consistent with the Kappabridge results, which show a loss of all magnetization in a similar temperature range (Figs 2d–f). The majority of the thermomagnetic curves for all sites except for 14/*R* appear largely reversible (Figs 2a and b, and d and e) suggesting no significant alteration to the samples is occurring up to temperatures of 600–700 °C. Samples from site 14/*R* show a slight increase in susceptibility between 500 and 600 °C and a relatively large increase between 600 and 700 °C (Figs 3c and f). The increase in susceptibility/magnetization with no associated change to the Curie Temperature suggests that magnetite is being created above 600 °C. The lack of alteration below 600 °C supports that the site could provide reliable palaeointensity estimates.

SEM images from example specimens for each of the sites suggest that most opaque grains contain intergrowths of ilmenite lamellae and magnetite with two different size distributions (Figs 2g and h). Larger iron oxide grains are subdivided by needles of ilmenite on the order of tens of μm long that are visible at the lower magnification (top row) and also smaller lamellae on the order of ≤ 1 μm that are only visible in the close-up images (bottom row). These structures are consistent with those observed from two-stage oxyexsolution processes (Gapeev & Tselmovich, 1983) and would be expected to yield an unbiased palaeointensity estimate even in the case of a high-temperature thermochemical remanence (Shcherbakov *et al.* 2019). The samples from sites 13/*R* (Fig. 2g) and 35/*R* show the lamellae in large, subhedral grains that have some cracks running through them. Cracks like these can represent a reduction in volume associated with maghematization of magnetite but it is unclear whether these cracks were caused by this as they appear similar to the cracks in other mineral grains in the image and there is little evidence of maghemite altering to haematite upon heating in the associated rock magnetic experiments (Figs 2a and d). The samples from sites 29/*R* (Fig. 2h) and 15/*R* show the lamellae dividing up skeletal grains and, in some cases, the grains show signs of pitting in the fine lamellae portions of the grain (Fig. 2h, bottom image). The SEM images for site 14/*R* (Fig. 2i) show a different texture, with what appears to be skeletal grains made up of ≤1 μm magnetite grains (top image). The accompanying EDX did not indicate any titanium to suggest the presence of ilmenite lamellae, although it is possible that ilmenite lamellae are present but are too small to be resolved by the SEM

The SEM images are consistent with the hysteresis properties of the samples determined from the MMVFTB and summarized on the Day plot (Day *et al.* 1977; Fig. 3). The bulk domain stability (BDS) trendline has been included (Paterson *et al.* 2017). The rock magnetic properties of samples plot in the upper part of the pseudo-single-domain (PSD, *sensu lato)* region, with most data clustering together, apart from 14/*R* which includes grains that appear substantially smaller than in other samples. The accompanying Arai plots (Fig. 4) are also fairly consistent with the hysteresis properties, with the Arai plots from site 14 showing less curvature due to a smaller overprint (Fig. 4b) than those from other sites.

PALAEOINTENSITY

Method

Several palaeointensity techniques were attempted to determine the strength of the geomagnetic field at 2.6 Ga. Thermal Thellier-type experiments, performed using the IZZI protocol (Tauxe & Staudigel 2004; Yu & Tauxe 2005) with partial thermal remanent magnetization (pTRM) checks (Coe 1967), were undertaken on 25-mm diameter core samples that were 12 mm in length. These experiments were performed at Curtin University using a TD-48-SC thermal demagnetizer, a 2 G Cryogenic magnetometer with a RAPID sample handling system (Kirschvink *et al.* 2008), and an Agico JR-6A spinner magnetometer. The heating steps were performed in air using an applied field strength of 20 or 30 μT parallel to the *Z*-axis of the

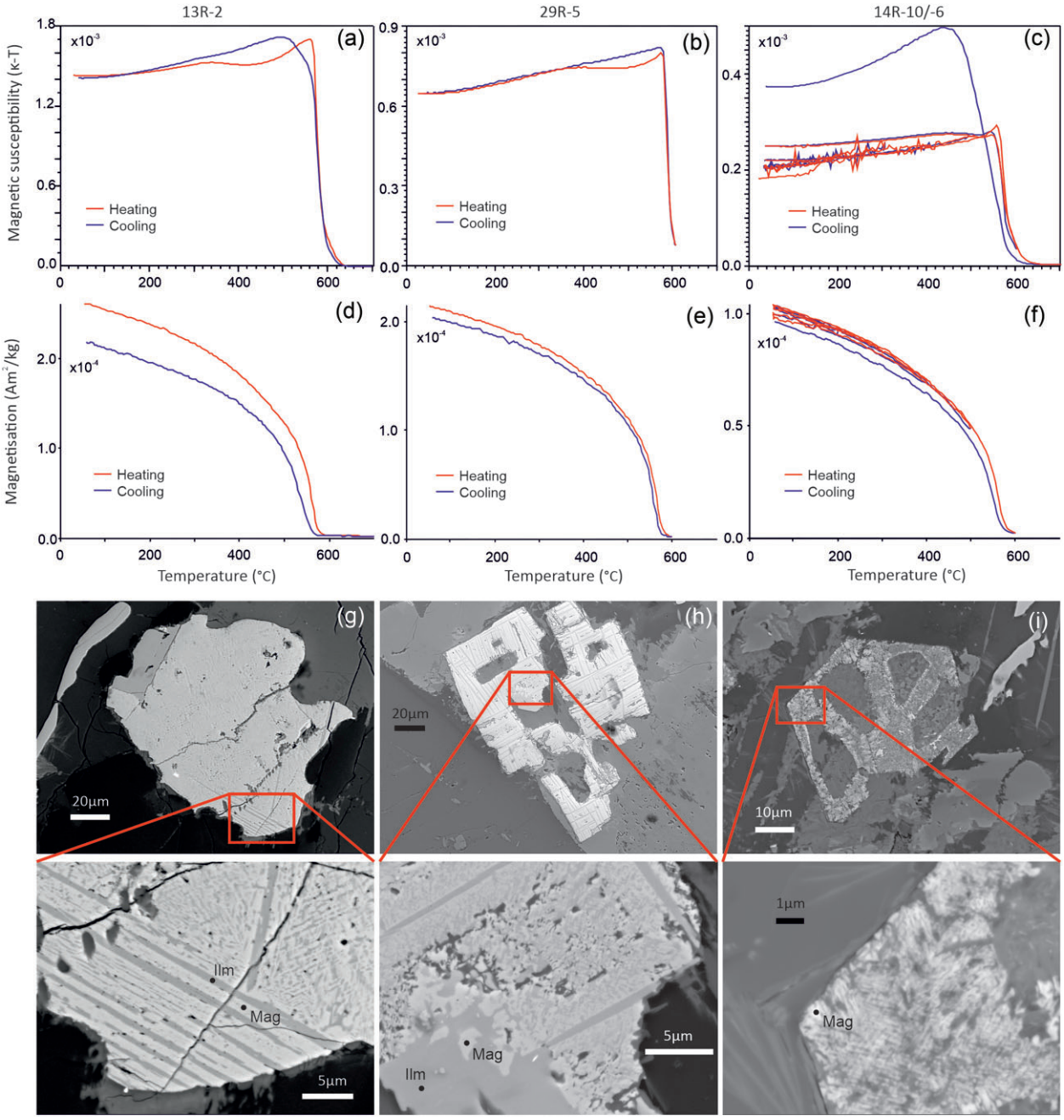

Figure 2. Representative rock magnetic properties and corresponding SEM images of the magnetic mineralogy for samples that gave results that passed selection criteria from cores 13*R*−2 (first column), 29*R*−5 (second column) and 14*R*−10/−6 (third column; the rock magnetic properties come from core 10 and the SEM images come from core 6, which shows similar behaviour). Thermomagnetic curves show (a)–(c) susceptibility versus temperature (κ–T; $\times 10^{-3}$) and (d)–(f) magnetization versus temperature ($Am^2\,kg^{-1}$; $\times 10^{-4}$); all samples were crushed and were measured in air. Backscattered electron (BSE) SEM images (g)–(i) illustrate the iron oxide textures present in these samples. The magnetic mineralogy was determined from EDX analysis: Mag, Magnetite (lighter grey) and Ilm, Ilmenite (darker grey).

core specimens. As the ChRM of these samples exists at temperatures $\geq 500\,^{\circ}C$, only 1–2 heating steps were included below this temperature. A heating step at 250 °C was included to allow for a pTRM check between 250 and 480–500 °C to identify low temperature alteration, that is, maghemite. Some of these thermal experiments also underwent low temperature demagnetization (LTD) by submerging the sample in liquid nitrogen three times and allowing it to warm in a shielded environment. This was done after every heating step in an attempt to remove multidomain (MD) remanence (Smirnov *et al.* 2017) by cooling the sample below the Verwey transition of magnetite (Verwey 1939). This did produce demagnetization up to several tens of per cent and the intention was to see if this improved the palaeointensity results. Experiments were also performed using microwave energy to demagnetize and remagnetize the samples, continuing with the IZZI protocol with pTRM checks (Th-IZZI+) and using the unique 14 GHz microwave palaeointensity system (Tristan) at the University of Liverpool (Hill & Shaw 1999; Suttie *et al.* 2010). The microwave experiments were performed in air,

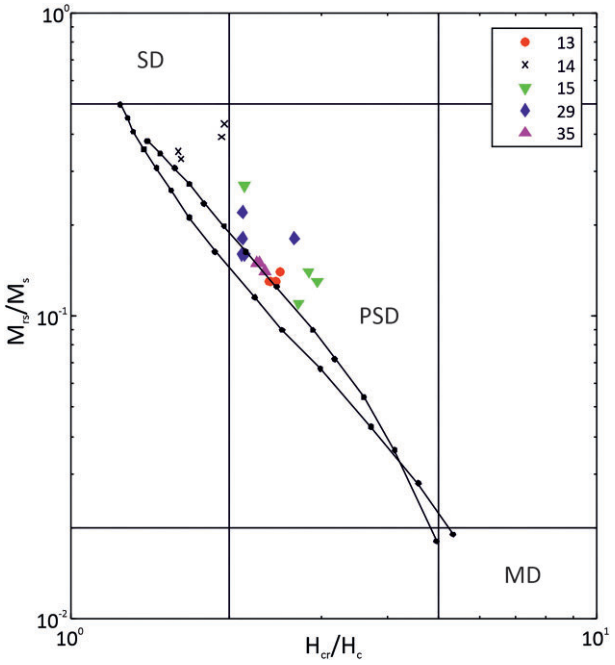

Figure 3. Day plot (Day *et al.* 1977) showing the hysteresis properties of samples that produced palaeointensity measurements that passed selection criteria from the resampled cores. Dashed line represents the BDS trendline (Paterson *et al.* 2017). Points are coded by site. Abbreviations are: Mrs, saturation remanence; Ms, saturation magnetization; Hc, coercivity; Hcr, coercivity of remanence; SD, single domain; PSD, pseudo-single domain and MD, multidomain.

on 5 mm diameter cores and with a field of 10 or 20 μT applied with at an angle $> 45°$ with respect to the NRM (natural remanent magnetisation).

All the Thellier-type experiments were evaluated using modified MC-CRIT.C1 selection criteria (Table 1) following (Paterson *et al.* 2015) and are described in greater detail in 'Standard Palaeointensity Definitions' (Paterson *et al.* 2014). This set of criteria has shown to successfully filter out biased palaeointensity estimates, even in the absence of pTRM tail checks (Grappone *et al.* 2019). Tail checks were not used here as we expect that MD behaviour would be expressed as zig-zagging in the Arai and/or orthogonal plot (Tauxe & Staudigel 2004). To further compensate for the lack of tail checks, the limit on the $|k'|$ statistic (Paterson 2011) was reduced to 0.36 in order to exclude Arai plots that are curved due to MD behaviour (Levi 1977). A further modification made to the MC-CRIT.C1 criteria was that the FRAC criterion was changed from ≥ 0.55 to ≥ 0.25 (consistent with Hawkins *et al.* 2019; Kodama *et al.* 2019). This reduction was due to the ChRM only being present at high unblocking temperatures ($\geq$500 °C), while MC-CRIT.C1 was developed for single component analysis. Alteration can also be issue where the ChRM exists at such high temperatures, so CDRAT′ and n_{pTRM} (Paterson *et al.* 2014) have also been added to reduce the risk of alteration affecting the palaeointensity estimates even further.

The double-heating technique (DHT) variant (Rolph & Shaw 1985; Tsunakawa & Shaw 1994) of the Shaw (1974) method was also performed. The experimental procedure and naming conventions used in this study are the same as those outlined in Yamamoto *et al.* (2003). Samples were AF demagnetized, measured, given an anhysteretic remanent magnetization (ARM) using an applied field of 1000 mT and demagnetized again using the AF (Alternating field) demagnetizer integrated into both the Curtin and Liverpool 2 G systems. The DHT technique then involves giving the sample a TRM twice with the same AF and ARM steps performed on the sample after each TRM acquisition. The TRM step was done either in Argon using the TD-48-SC or under vacuum using the MMTD24 thermal demagnetizers at Curtin and Liverpool, respectively. During the TRM step, samples were heated to 600 °C and held for 20 min for TRM1 and 60 min for TRM2, while a field of 20 μT was applied parallel to the *z*-axis of the half cores. The palaeointensity is calculated from the ratio of NRM to TRM1∗ (TRM1 corrected using a ratio of ARM0/ARM1), from the selected linear component of the NRM-TRM1∗ plot. For analysis of the Shaw-type experiments, the selection criteria used are the same as those used in Yamamoto *et al.* (2003) plus the $\mathrm{MAD}_{\mathrm{ANC}}$ and α criterion determined in the same way as for the Thellier criteria (see Table 1).

Results

A total of 122 samples across 11 sites were measured for palaeointensity, with 28 measurements from 6 sites accepted, giving a pass rate of 23 per cent. A summary of all palaeointensity results and associated parameters are provided in the Supporting Information (Tables S1 and S2). The site mean results, which range from 5.9 to 26.3 μT (virtual dipole moment, VDM's of 11–44 ZAm^2) are provided in Table 2. Of the accepted measurements, the majority (54 per cent) came from microwave experiments, 29 per cent came from the Shaw experiments and 18 per cent from the thermal Thellier experiments. None of the LTD-Shaw experiments passed the selection criteria of Yamamoto *et al.* (2003). While two of the LTD-Thermal experiments passed the selection criteria outlined in Table 1, they were lower than expected, in direct opposition to what is expected from the application of LTD steps (Smirnov *et al.* 2017). There was some suspicion that other factors may have resulted in these results being biased unexpectedly, possibly due to oxidation or the presence of titanium affecting the Verwey (1939) transition, and therefore they were excluded. The majority of the accepted Arai plots (Fig. 4) from both the thermal and microwave experiments showed two components with distinct directions on the accompanying orthogonal plots. In some cases (e.g. site 14/*R*; Fig. 4b), there was little unblocking until high temperatures/powers and only a single stable component was observed. Representative examples of some of the accepted Shaw results (Fig. 5) also show linear selected components, corresponding to the ChRM direction. The most common selection criteria the Thellier-type experiments failed were β or DRAT, suggesting experiments either failed because of large PSD to MD behaviour or alteration. While many of the samples that provided reliable palaeointensity estimates, it is clear from the SEM analysis (Fig. 2) and the hysteresis properties of the samples (Fig. 3), that most of the samples include larger magnetite grains that can produce non-ideal behaviour. As for alteration, the ChRM is generally only present at high unblocking temperatures (~550–580 °C), with alteration occurring close to the Curie temperature of magnetite causing the last pTRM checks to fail. The small temperature range may explain why there is a greater success rate for the microwave experiments than the thermal one as the microwave technique can cause less alteration then comparative thermal experiments (e.g. Grappone *et al.* 2020). For the Shaw experiments, the overprint and the ChRM do not always unblock as cleanly as in the thermal experiments, making the selectable ChRM component smaller.

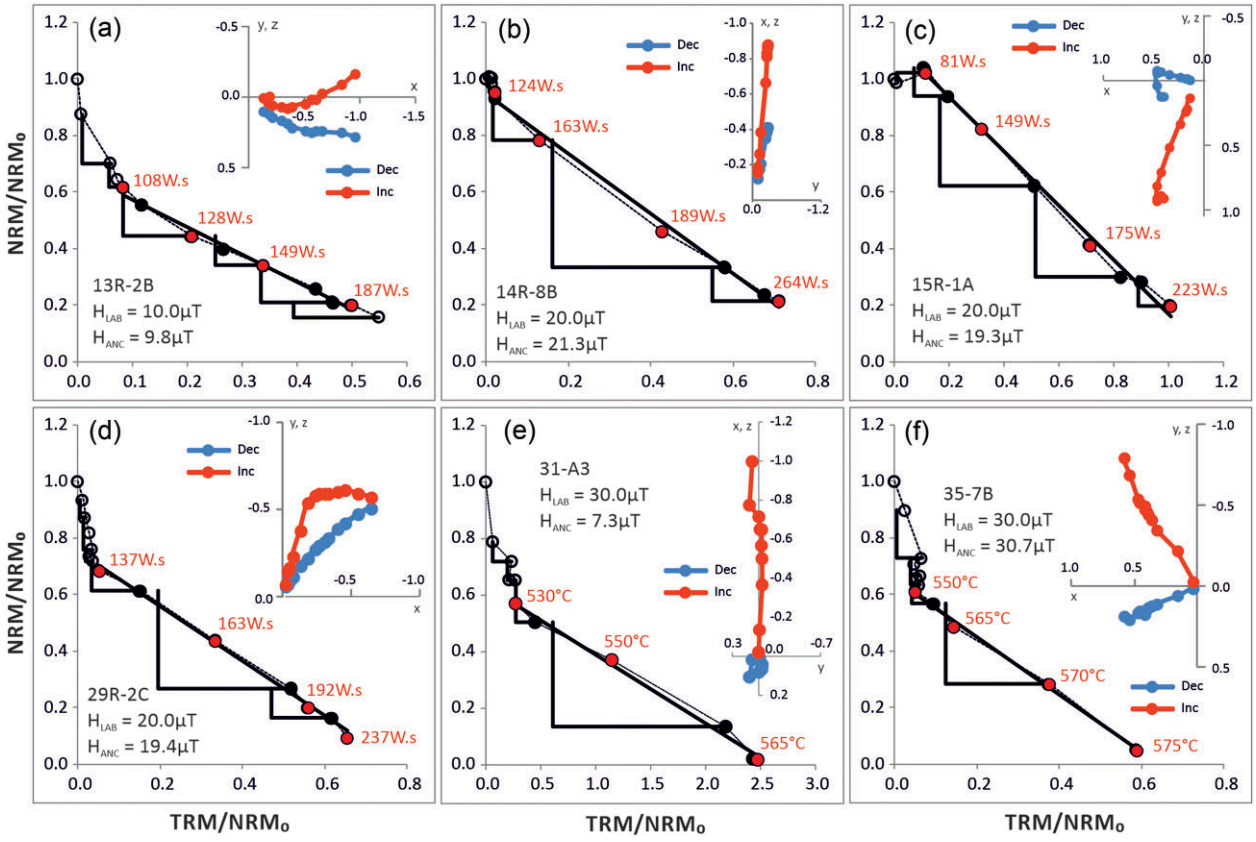

Figure 4. Representative accepted Arai plots from example Thellier-type experiments, one from each site, with accompanying orthogonal plots. (a)–(d) Microwave, and (e) and (f) thermal Thellier plots. The black line and filled in circles represent the selected component, with red fill circles showing the power integral (Watts per second; W·s) or temperature (°C) of the step. H_{LAB} is the strength of the applied field used during in-field steps and pTRM checks and H_{ANC} is the palaeointensity estimate derived from the plot.

Table 1. Selected criteria applied to all of the Theiler-type measurements (thermal and microwave), modified from the MC-CRIT.C1 criteria (Paterson *et al.* 2015). Details of all of the selection criteria are listed in the standard palaeointensity definitions accompanying Paterson *et al.* (2014).

n	β	FRAC	q	DRAT	|CDRAT'|	MAD_{ANC}	α	$\lvert\overrightarrow{k}\rvert$	n_{pTRM}
≥ 4	≤ 0.1	≥ 0.25	≥ 4	$\leq 10\%$	$\leq 10\%$	≤ 10	≤ 10	0.36	≥ 3

Table 2. Summary of the site mean palaeodirections (Liu *et al.* 2021) palaeointensity data, and Q_{PI} assessment. Abbreviations are: n_D/N_D, number of directions measured/number of directions accepted; $n/N_T/N_S/N_{MW}/N$, total number of palaeointensity measurements/number of thermal that passed selection criteria/number of Shaw that passed/number of microwave that passed/total number of measurements that passed; PI, palaeointensity; s.d., standard deviation; VDM, virtual dipole moment and Q_{PI} criteria as defined in Biggin & Paterson (2014), Biggin *et al.* (2015) and Kulakov *et al.* (2019).

Site	Lat (°S)	Long (°E)	Palaeodirections (stratigraphic)					Palaeointensity					Q_{PI} criteria									
			n_D/N_D	Dec.	Inc.	k	a95	$n/N_T/N_S/N_{MW}/N$	PI (μT)	s.d. (μT)	s.d./ PI (per cent)	VDM (ZAm^2)	AGE	DIR	STAT	TRM	ALT	MD	ACN	TECH	LITH	MAG	Q_{PI}
13/*R*	32.1	117.2	8/6	295.9	−51.0	24.0	15.5	22/1/2/2/5	7.1	1.7	24	14	1	0	0	1	1	1	1	1	0	1	7
14/*R*	31.6	116.9	9/8	277.9	−56.7	33.0	10.0	21/0/2/2/4	20.1	1.0	5	36	1	0	0	1	1	1	1	1	0	1	7
15/*R*	31.5	116.9	10/6	287.8	−59.6	50.0	9.6	23/0/1/4/5	25.8	6.6	26	44	1	1	0	1	1	1	1	1	0	1	8
29/*R*	31.6	116.9	9/9	292.7	−58.3	57.0	6.9	30/1/1/4/6	22.1	7.9	36	39	1	1	0	1	1	1	1	1	0	1	8
31	31.6	116.9	8/6	290.9	−50.3	65.0	8.5	8/2/0/0/2	5.9	2.1	35	11	1	1	0	1	1	1	1	0	0	1	7
35/*R*	31.8	117.4	8/8	304.6	−63.9	36.0	9.4	18/1/2/3/6	26.3	4.8	18	43	1	0	0	1	1	1	1	1	0	1	7

DISCUSSION

To assess the reliability of the site level results, the nine qualitative palaeointensity (Q_{PI}) criteria outlined by Biggin & Paterson (2014) and Biggin *et al.* (2015) were evaluated for each site and are summarized in Table 2. All of the sites passed AGE as there are isotopic age constraints (Stark *et al.* 2018) and palaeodirections were determined from origin-trending, high temperature components that contributed to an accepted palaeomagnetic pole (Liu *et al.* 2021). Three of the sites passed DIR as the directions came from ≥ 5 samples and have a Fisher (1953) precision parameter $k \geq 50$. None of the sites pass STAT ($n \geq 5$ and standard deviation equivalent to 25 per cent based on Paterson *et al.* 2010). All the sites except site 31 have had SEM analysis performed on representative specimens from them. These SEM images show fine magnetite lamellae consistent with primary exsolution textures and no conclusive evidence for maghematization. The successful Arai plots from site 31 looked similar to those from others and there was no suspicion that these images were not also representative of site 31. Samples showing

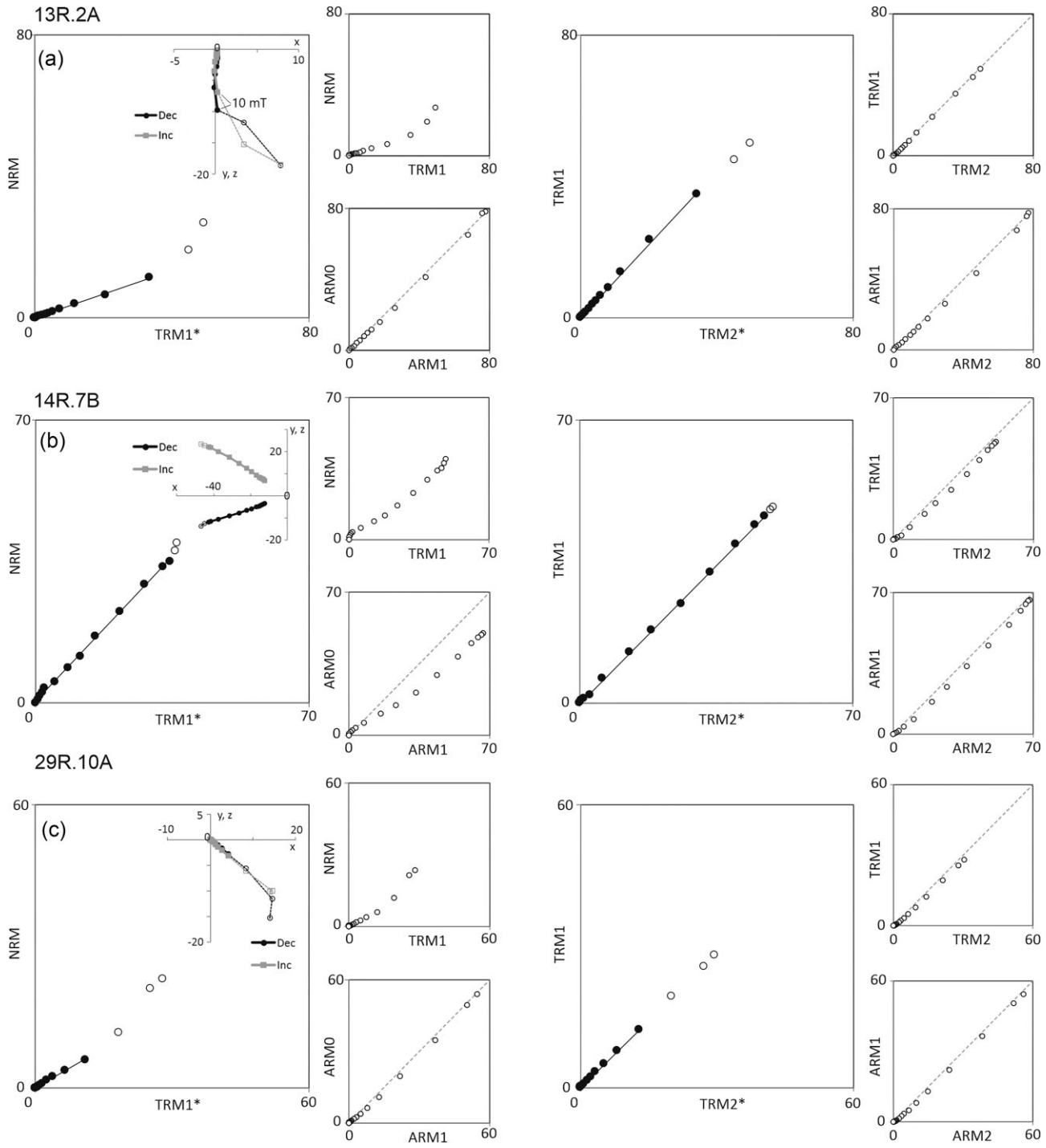

Figure 5. Representative plots from accepted DHT Shaw experiments with accompanying orthogonal plots. The black line and filled in circles represent the selected component. NRM, TRM1/2 and ARM0/1/2 represent the AF demagnetization data along the axis for each of these steps as described in Yamamoto *et al.* (2003), while TRM1/2∗ are the ARM corrected data from TRM1/2. The intensity of the magnetization for all of the plots is given in A m^{-1}.

a bimodal magnetite grain size distribution formed through two-stage oxyexsolution, with the smaller lamellae potentially forming just below the Curie temperature of magnetite (Gapeev & Tselmovich 1983). In this case, the ChRM could be thermochemical remanent magnetization (TCRM). Despite this, it has been shown that artificially produced TCRMs acquired just below the Curie temperature yield unbiased palaeointensity results (Shcherbakov *et al.* 2019). Given the high unblocking temperature range of the ChRM of the YDS samples, these palaeointensity results should also be unbiased by this phenomenon. We therefore consider the spirit of the TRM criterion to have been met by all of our results. All of the sites pass ALT as the Thellier-type experiments included pTRM checks with appropriate DRAT/CDRAT selection criteria and the Shaw experiments used an ARM correction, also subject to strict criteria. All sites also pass MD as the IZZI protocol was used on the Thellier-type experiments and produced no visual evidence of the

zig-zagging (Yu & Tauxe 2005). Furthermore, a check for the curvature of the selected component ($|\vec{k}'|$) (Paterson 2011) was made. Finally, the Shaw method is expected to be domain-state independent because it uses full TRMs. All the three parts of ACN are also passed. First, we use measurements of Υ (the angle between the last pTRM and the applied field direction) to detect the presence of anisotropy of TRM. This was found to be $< 6^\circ$ for all the accepted measurements suggesting that its presence was small and unlikely to significantly bias the palaeointensity estimates. The second part, cooling rate, is also not considered to be problematic as the magnetic carriers are likely to be vortex-state rather than non-interacting SD, based on the hysteresis properties (Fig. 3) and the SEM images (Figs 2g–i). Such grain sizes are not anticipated to produce substantial cooling rate effects (Biggin *et al.* 2013). Cooling rates used in the Shaw and microwave experiments differed by roughly two orders of magnitude (Poletti *et al.* 2013) but the resulting palaeointensities were indistinguishable, supporting our assumption that cooling differences between nature and the lab are unlikely to have severely biased our results. The last part of ACN is nonlinearity and this should not affect these results as the majority of estimates and applied field values are within 1.5 times of each other and all are well below the field values known to cause substantial nonlinearity issues (60 μT, Selkin *et al.* 2007). All the sites, apart from site 31, pass TECH because they include more than one technique with a different mode of unblocking magnetic grains (ie. thermal, microwave and AF). None of the sites pass LITH as only a single lithology was measured throughout. All data have been uploaded to MagIC (https://www2.earthref.org/MagIC) at the measurement level and therefore the MAG criterion is also met. While this criterion does not address the technical quality of palaeointensity estimates, we strongly promote its use. This is because we consider that measurement data that adhere to FAIR principles (findable, accessible, interoperable and reusable) are intrinsically more reliable because they are far more amenable to re-analysis and falsification.

The various criteria applied suggest that the results from the YDS are reliable and yield a mean VDM of 37 ± 15 ZAm^2 (± 1 standard deviation) at 2.62 Ga. This value, approximately half that of the present day, is not entirely in accord with the predictions of some thermal evolution models (Bono *et al.* 2019; Davies *et al.* 2022). Such models tend to predict a strong field at 2.6 Ga which then decays through the Palaeo- and Neo-Proterozoic, reaching a minimum just ahead of ICN between 500 and 900 Ma. Nevertheless, care must be taken in considering any set of results in isolation. We cannot be certain to have captured a reasonable representation of secular variation in these results. Even if we have, the difference in field strength between the expected values from thermal evolution models and results from sites that are relatively close in age (Fig. 6) may reflect variation occurring on timescales of tens of millions of years, similar to that observed during the Phanerozoic (Kulakov *et al.* 2019; Hawkins *et al.* 2021) and Neoproterozoic (Lloyd *et al.* 2021; Thallner *et al.* 2022), potentially biasing our understanding of average Precambrian field strength.

In Fig. 6(a), we plot the new estimates together with all published VDM and virtual axial dipole moment (VADM) measurements associated with Q_{PI} values ≥ 3 from rocks with ages between 2.3 and 2.8 Ga. There is a large dispersion in estimates of similar ages which, assuming the data are trustworthy, could result from the effects of secular variation (on timescales <1 Myr) and from longer timescale variations (~10–100 Myr) as a consequence of variable mantle forcing of the geodynamo (Biggin *et al.* 2012). One measure of the relative variance of a group of V(A)DMs was defined by Sprain *et al.* (2019) as:

$$V \text{ per cent} = \hat{\mathrm{VDM}}/\mathrm{VDM}_{\mathrm{med}}$$

where $\hat{\mathrm{VDM}}$ is the interquartile range and $\mathrm{VDM}_{\mathrm{med}}$ is the median value for a set of VDM values. V per cent has a value of 57 per cent for the interval assessed here (Fig. 6b). To put the Archaean/earliest Proterozoic observations into context and allow for an assessment of very long term (~2 Gyr) changes in dipole moment, we show the equivalent plots for the most part of the Phanerozoic (10–500 Ma, Figs 6c and d). Fig. 6(c) allows the dipole lows in the mid-Jurassic (Kulakov *et al.* 2019) and mid-Palaeozoic (Hawkins *et al.* 2021) to be clearly discerned. It further invites the possibility of there being similar intervals in Precambrian interval studied and demonstrates that the data density is simply not high enough to infer them. A comparison of the distributions of dipole moment data for the two intervals suggests that they may not otherwise be identical, however. While their averages are close to equal, the distribution of the 10–500 Ma data is more strongly skewed to low values and has substantially enhanced variance (as reflected in its significantly higher interquartile range and V per cent; Figs 6b and d). A two-sample Kolmogorov–Smirnov test excludes the null hypothesis of identical distributions with 95 per cent confidence ($P = 0.03$).

The analysis above supports that the variance of dipole moment measurements from rocks dated between 2.3 and 2.8 Ga was significantly smaller than that that from rocks dated between 10 and 500 Ma. Such variance arises from time variations in the magnetic field intensity and direction and the differences suggest that these variations were suppressed in the earlier time period. Based on this observed difference, we hypothesize that the geodynamo at 2.5 Ga was in state conducive to producing a global field that was neither much stronger nor much weaker on average than the Phanerozoic, but rather more stable through time. We stress that this does not preclude the possibility of variations on mantle timescales similar to the Phanerozoic but supports that these and/or unforced secular variation were somewhat milder. Interestingly, directional palaeosecular variation has also been argued to have been suppressed in the late Archaean—earliest Proterozoic relative to later times including the last few hundreds of Myr (Biggin *et al.* 2008; Smirnov *et al.* 2011; Veikkolainen & Pesonen 2014). Suppressed equatorial dispersion of virtual geomagnetic poles translates directly into enhanced axial dipole dominance (Biggin *et al.* 2020), although the associated uncertainties are large. We speculate that the geomagnetic field in the late Archaean–earliest Proterozoic was more stably dipolar and less susceptible to collapse, perhaps resulting in fewer polarity reversals (Coe & Glatzmaier 2006), than the Phanerozoic field, while maintaining a similar average dipole moment.

CONCLUSIONS

The YDS has been shown to be suitable for providing reliable palaeointensity estimates with associated Q_{PI} scores of 7 or 8 from a total of 10. The six accepted sites from the YDS give site mean values of 5.9–26.3 μT, which convert to VDM values of 11–44 ZAm^2. These values fit well with the average for the entire interval 2300–2800 Ma, which now has more than 100 dipole moment estimates with $Q_{\mathrm{PI}} \geq 3$. Compared with the similarly long Phanerozoic era, the dipole field in the late Archaean–earliest Proterozoic appears to have been similar in average strength but less prone to exhibit variability in its magnitude. This provides a constraint on thermal evolution models for the early Earth and would seem to rule

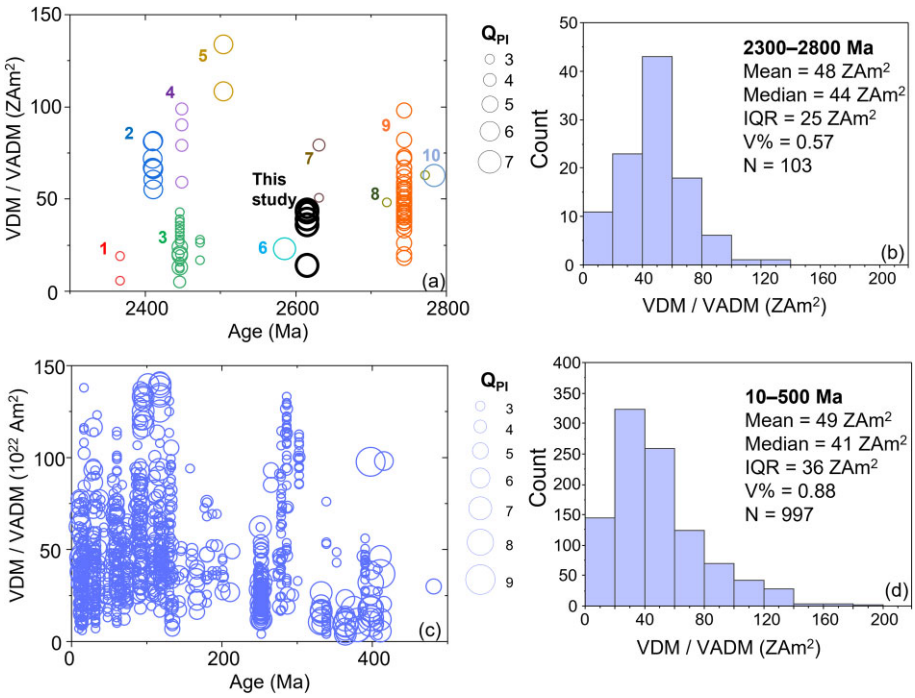

Figure 6. Comparison of dipole moment estimates in interval 2300–2800 Ma and 10–500 Ma taken from PINT v8.1 (Bono *et al.* 2022). (a) and (c) Time-series of estimates with circle size denoting Q_{PI} value (Biggin & Paterson 2014). Published estimates in (a) are taken from (1) Dharwar Dykes (Valet *et al.* 2014); (2) Widgiemooltha Dykes (Smirnov & Evans 2015); (3) Matachewan Dyke Swarm (Macouin *et al.* 2003; Halls *et al.* 2004; Smirnov & Tarduno 2005; Smirnov *et al.*, 2005); (4) Karelia Dykes (Smirnov *et al.* 2003); (5) Vodlozerskii Terrane Dykes (Shcherbakova *et al.* 2017); (6) Nuuk Dyke (Morimoto *et al.* 1997); (7) Slave Dykes (Yoshihara & Hamano 2000); (8) Pilbara Lavas (Biggin *et al.* 2009); (9) Stillwater Complex (Selkin *et al.* 2008) and (10) Modipe Gabbro (Muxworthy *et al.* 2013). (b) and (d) Histograms and summary statistics of dipole moment estimates from the two intervals. Note that all estimates denoted as transitional polarity were omitted.

out those that predict a substantially stronger or weaker field in the Archaean than in the Phanerozoic.

ACKNOWLEDGMENTS

This study was a consequence of a NERC global partnerships seed-corn fund grant awarded to AJB and ZXL (NE/S008330/1). LH and AJB acknowledge further funding from the Natural Environment Research Council (NE/P00170X/1). AJB and JMG acknowledge funding from The Leverhulme Trust (RLA-2016–080). ZXL and AJB acknowledge funding from the Australian Research Council (DP210102495). ZXL further acknowledge the Australian Research Council for Laureate Fellowship grant (FL150100133). We thank Richard Bono (Florida State University) for comments and edits made to this manuscript. We thank Valentina Shcherbakova, Evgeniy Kulakov and Yo-ichiro Otofuji for detailed and thoughtful reviews that substantially improved the manuscript. LH measured, processed, analysed and interpreted the new data and wrote the first draft of the manuscript. AB performed the meta-analysis, wrote a later draft of the manuscript, and co-initiated the project. YL and JMG assisted with the analysis and writing of the manuscript. ZXL assisted with the writing of the manuscript and co-initiated the project.

DATA AVAILABILITY

All palaeomagnetic data have been uploaded to the MagIC database (earthref.org/MagIC/19619) and have the data DOI: 10.7288/V4/MAGIC/19619.

SUPPORTING INFORMATION

Supplementary data are available at *GJI* online.

Please note: Oxford University Press is not responsible for the content or functionality of any supporting materials supplied by the authors. Any queries (other than missing material) should be directed to the corresponding author for the paper.

REFERENCES

Aubert, J., Labrosse, S. & Poitou, C., 2009. Modelling the palaeo-evolution of the geodynamo. *Geophys. J. Int.,* **179,** 1414–1428. 10.1111/j.1365-246X.2009.04361.x.

Badro, J., Siebert, J. & Nimmo, F., 2016. An early geodynamo driven by exsolution of mantle components from Earth's core. *Nature,* **536,** 326–328. 10.1038/nature18594.

Biggin, A.J., Badejo, S., Hodgson, E., Muxworthy, A.R., Shaw, J. & Dekkers, M.J., 2013. The effect of cooling rate on the intensity of thermoremanent magnetization (TRM) acquired by assemblages of pseudo-single domain, multidomain and interacting single-domain grains. *Geophys. J. Int.,* **193,** 1239–1249. 10.1093/gji/ggt078.

Biggin, A.J., Bono, R.K., Meduri, D.G., Sprain, C.J., Davies, C., Holme, R. & Doubrovine, P.V., 2020. Quantitative estimates of average geomagnetic axial dipole dominance in deep geological time. *Nat. Commun.,* **11,** 6100. 10.1038/s41467-020-19794-7.

Biggin, A.J., de Wit, M.J., Langereis, C.G., Zegers, T.E., Voute, S., Dekkers, M.J. & Drost, K., 2011. Palaeomagnetism of Archaean rocks of the Onverwacht Group, Barberton Greenstone Belt (southern Africa): evidence for a stable and potentially reversing geomagnetic field at ca. 3.5 Ga. *Earth planet. Sci. Lett.,* **302,** 314–328. 10.1016/j.epsl.2010.12.024.

Biggin, A.J. & Paterson, G.A., 2014. A new set of qualitative reliability criteria to aid inferences on palaeomagnetic dipole moment variations through geological time. *Front. Earth Sci.,* **2** (24), 21–29.

Biggin, A.J., Piispa, E.J., Pesonen, L.J., Holme, R., Paterson, G.A., Veikkolainen, T. & Tauxe, L., 2015. Palaeomagnetic field intensity variations suggest Mesoproterozoic inner-core nucleation. *Nature,* **526,** 245–248. 10.1038/nature15523.

Biggin, A.J., Steinberger, B., Aubert, J., Suttie, N., Holme, R., Torsvik, T.H., van der Meer, D.G. & van Hinsbergen, D.J.J., 2012. Possible links between long-term geomagnetic variations and whole-mantle convection processes. *Nat. Geosci.,* **5,** 526–533. 10.1038/ngeo1521.

Biggin, A.J., Strik, G. & Langereis, C.G., 2009. The intensity of the geomagnetic field in the late-Archaean: new measurements and an analysis of the updated IAGA palaeointensity database. *Earth Planets Space,* **61,** 9–22. 10.1186/BF03352881.

Biggin, A.J., Strik, G.H.M.A. & Langereis, C.G., 2008. Evidence for a very-long-term trend in geomagnetic secular variation. *Nat. Geosci.,* **1,** 395–398. 10.1038/ngeo181.

Bono, R.K., Paterson, G. & Biggin, A., 2022. MCADAM: a continuous paleomagnetic dipole moment model for at least 3.7 billion years. *Geophys. Res. Lett.,* **49,** e2022GL100898. 10.1002/essoar.10512285.1.

Bono, R.K., Tarduno, J.A., Nimmo, F. & Cottrell, R.D., 2019. Young inner core inferred from Ediacaran ultra-low geomagnetic field intensity. *Nat. Geosci.,* **12,** 143–147. 10.1038/s41561-018-0288-0.

Braginsky, S., 1963. Structure of the F layer and reasons for convection in the Earth's core. *Dokl. Acad. Nauk. SSSR (Eng. transl.),* **149 ,** 1311–1314.

Buffett, B.A., Huppert, H.E., Lister, J.R. & Woods, A.W., 1996. On the thermal evolution of the Earth's core. *J. geophys. Res.—Solid Earth,* **101,** 7989–8006. 10.1029/95JB03539.

Champion, D.C. & Sheraton, J.W., 1997. Geochemistry and Nd isotope systematics of Archaean granites of the Eastern Goldfields, Yilgarn Craton, Australia: implications for crustal growth processes. *Precambrian Res.,* **83,** 109–132. 10.1016/S0301-9268(97)00007-7.

Coe, R.S., 1967. Palaeointensities of the Earth's magnetic field determined from Tertiary and Quaternary rocks. *J. geophys. Res.—Solid Earth,* **72,** 3247–3262. 10.1029/JZ072i012p03247.

Coe, R.S. & Glatzmaier, G.A., 2006. Symmetry and stability of the geomagnetic field. *Geophys. Res. Lett.,* **33,** 2006GL027903. 10.1029/2006GL027903.

Davies, C., Bono, R.K., Meduri, D.G., Aubert, J., Greenwood, S. & Biggin, A.J., 2022. Dynamo constraints on the long-term evolution of Earth's magnetic field strength. *Geophys. J. Int.,* **228,** 316–336. 10.1093/gji/ggab342.

Davies, C., Pozzo, M., Gubbins, D. & Alfe, D., 2015. Constraints from material properties on the dynamics and evolution of Earth's core. *Nat. Geosci.,* **8,** 678–685. 10.1038/ngeo2492.

Day, R., Fuller, M. & Schmidt, V. A., 1977. Hysteresis properties of titanomagnetites: grain-size and compositional dependence, *Physics of the Earth and Planetary Interiors,* **13,** 260–267. 10.1016/0031-9201(77)90108-X.

Fisher, R. A., 1953. Dispersion on a sphere, *Proceedings of the Royal Society of London,* **A217,** 295–305. 10.1098/rspa.1953.0064.

Gapeyev, A. & Tselmovich, V., 1983. The microtexture of synthetic titanomagnetite oxidized at high partial pressure of oxygen, *Izv. Akad. Nauk SSSR, Fiz Zemli,* **12,** 91–95.

Grappone, J. M., Biggin, A. J., Barrett, T. J., Hill, M. J. & Sprain, C. J., 2020. Comparison of Thermal and Microwave Paleointensity Estimates in Specimens Displaying Non-Ideal Behavior in Thellier-Style Paleointensity Experiments, **125**(), e2020JB019802.

Grappone, J.M., Biggin, A.J. & Hill, M.J., 2019. Solving the mystery of the 1960 Hawaiian lava flow: implications for estimating Earth's magnetic field. *Geophys. J. Int.,* **218,** 1796–1806. 10.1093/gji/ggz252.

Halls, H.C., McArdle, N.J., Gratton, M.N., Hill, M.J. & Shaw, J., 2004. Microwave paleointensities from dyke chilled margins: a way to obtain long-term variations in geodynamo intensity for the last three billion years. *Phys. Earth planet. Inter.,* **147,** 183–195. 10.1016/j.pepi.2004.03.013.

Hawkins, L., Anwar, T., Shcherbakova, V.V., Biggin, A.J., Kravchinsky, V.A., Shatsillo, A. & Pavlov, V., 2019. An exceptionally weak Devonian geomagnetic field recorded by the Viluy Traps, Siberia. *Earth planet. Sci. Lett.,* **506,** 134–145. 10.1016/j.epsl.2018.10.035.

Hawkins, L., Grappone, J.M., Sprain, C.J., Saengduean, P., Sage, E.J., Thomas-Cunningham, S., Kugabalan, B. & Biggin, A.J., 2021. Intensity of the Earth's magnetic field: evidence for a Mid-Paleozoic dipole low. *Proc. Natl. Acad. Sci. USA,* **118,** e2017342118. 10.1073/pnas.2017342118.

Hill, M.J. & Shaw, J., 1999. Palaeointensity results for historic lavas from Mt Etna using microwave demagnetization/remagnetization in a modified Thellier-type experiment. *Geophys. J. Int.,* **139,** 583–590. 10.1046/j.1365-246x.1999.00980.x.

Kent, A.J.R., Cassidy, K.F. & Mark Fanning, C., 1996. Archean gold mineralization synchronous with the final stages of cratonization, Yilgarn Craton, Western Australia. *Geology,* **24,** 879–882. 10.1130/0091-7613(1996)0242.3.CO;2.

Kirschvink, J. L., Kopp, R. E., Raub, T. D., Baumgartner, C. T. & Holt, J. W., 2008. Rapid, precise, and high-sensitivity acquisition of paleomagnetic and rock-magnetic data: Development of a low-noise automatic sample changing system for superconducting rock magnetometers, *Geochemistry, Geophysics, Geosystems,* **9**(5), 10.1029/2007GC001856.

Kodama, K.P., Carnes, L.K., Tarduno, J.A. & Berti, C., 2019. Palaeointensity of the 1.3 billion-yr-old Gardar basalts, southern Greenland revisited: no evidence for onset of inner core growth. *Geophys. J. Int.,* **217,** 1974–1987. 10.1093/gji/ggz126.

Kulakov, E.V., Sprain, C.J., Doubrovine, P.V., Smirnov, A.V., Paterson, G.A., Hawkins, L., Fairchild, L. & Biggin, A.J., 2019. Analysis of an updated paleointensity database (QPI-PINT) for 65-200 Ma: implications for the long-term history of dipole moment through the Mesozoic., *J. geophys. Res.—Solid Earth,* **124,** 9999–10022. 10.1029/2018JB017287.

Labrosse, S., 2015. Thermal evolution of the core with a high thermal conductivity. *Phys. Earth planet. Inter.,* **247,** 36–55. 10.1016/j.pepi.2015.02.002.

Landeau, M., Aubert, J. & Olson, P., 2017. The signature of inner-core nucleation on the geodynamo. *Earth planet. Sci. Lett.,* **465,** 193–204. 10.1016/j.epsl.2017.02.004.

Landeau, M., Fournier, A., Nataf, H.-C., Cébron, D. & Schaeffer, N., 2022. Sustaining Earth's magnetic dynamo. *Nat. Rev. Earth Environ.,* **3,** 255–269. 10.1038/s43017-022-00264-1.

Le Bars, M., Wieczorek, M.A., Karatekin, Ö., Cébron, D. & Laneuville, M., 2011. An impact-driven dynamo for the early Moon. *Nature,* **479,** 215–218. 10.1038/nature10565.

Levi, S., 1977. The effect of magnetite particle size on palaeointensity determinations of the geomagnetic field., *Phys. Earth planet. Inter.,* **13,** 245–259. 10.1016/0031-9201(77)90107-8.

Liu, Y., Mitchell, R.N., Li, Z.-X., Kirscher, U., Pisarevsky, S.A. & Wang, C., 2021. Archean geodynamics: ephemeral supercontinents or long-lived supercratons. *Geology,* **49,** 794–798. 10.1130/G48575.1.

Lloyd, S.J., Biggin, A.J. & Li, Z.X., 2021. New paleointensity data suggest possible phanerozoic-type paleomagnetic variations in the precambrian. *Geochem. Geophys. Geosyst.,* **22,** e2021GC009990. 10.1029/2021GC009990.

Lloyd, S.J., Biggin, A.J., Paterson, G.A. & McCausland, P.J.A., 2022. Extremely weak early Cambrian dipole moment similar to Ediacaran: evidence for long-term trends in geomagnetic field behaviour?, *Earth planet. Sci. Lett.,* **595,** 117757. 10.1016/j.epsl.2022.117757.

Macouin, M., Valet, J.P., Besse, J., Buchan, K., Ernst, R., LeGoff, M. & Scharer, U., 2003. Low paleointensities recorded in 1 to 2.4 Ga Proterozoic dykes, Superior Province, Canada. *Earth planet. Sci. Lett.,* **213,** 79–95. 10.1016/S0012-821X(03)00243-7.

McFadden, P.L. & McElhinny, M.W., 1990. Classification of the reversal test in palaeomagnetism. *Geophys. J. Int.,* **103,** 725–729. 10.1111/j.1365-246X.1990.tb05683.x.

McFarlane, C.R.M., 2010. *Geodynamic Constraints on Mineralization and Metamorphism at the Griffin's Find Gold Deposit,* Western Australia, from calibrated T-t trajectories. https://geoconvention.com/wp-content/uploads/abstracts/2010/0758_GC2010_Geodynamic_Constraints_on_Mineralization.pdf.

Mittal, T., Knezek, N., Arveson, S.M., McGuire, C.P., Williams, C.D., Jones, T.D. & Li, J., 2020. Precipitation of multiple light elements to power Earth's early dynamo. *Earth planet. Sci. Lett.,* **532,** 116030. 10.1016/j.epsl.2019.116030.

Morimoto, C., Otofuji, Y., Miki, M., Tanaka, H. & Itaya, T., 1997. Preliminary palaeomagnetic results of an Archaean dolerite dyke of west Greenland: geomagnetic field intensity at 2.8 Ga. *Geophys. J. Int.,* **128,** 585–593. 10.1111/j.1365-246X.1997.tb05320.x.

Muxworthy, A.R., Evans, M.E., Scourfield, S.J. & King, J.G., 2013. Paleointensity results from the late-Archaean Modipe Gabbro of Botswana. *Geochem. Geophys. Geosyst.,* **14,** 2198–2205. 10.1002/ggge.20142.

Nemchin, A.A. & Pidgeon, R.T., 1997. Evolution of the darling range batholith, Yilgarn Craton, Western Australia: a SHRIMP zircon study. *J. Petrol.,* **38,** 625–649. 10.1093/petroj/38.5.625.

O'Rourke, J.G. & Stevenson, D.J., 2016. Powering Earth's dynamo with magnesium precipitation from the core. *Nature,* **529,** 387–389. 10.1038/nature16495.

Paterson, G. A., Muxworthy, A. R., Yamamoto, Y. & Pan, Y., 2017. Bulk magnetic domain stability controls paleointensity fidelity, *Proceedings of the National Academy of Sciences,* **114**(), 13120–13125.

Paterson, G.A., 2011. A simple test for the presence of multidomain behavior during paleointensity experiments. *J. geophys. Res.—Solid Earth,* **116,** B10104. 10.1029/2011jb008369.

Paterson, G.A., Biggin, A.J., Hodgson, E. & Hill, M.J., 2015. Thellier-type paleointensity data from multidomain specimens. *Phys Earth planet. Inter.,* **245,** 117–133. 10.1016/j.pepi.2015.06.003.

Paterson, G.A., Heslop, D. & Muxworthy, A.R., 2010. Deriving confidence in paleointensity estimates. *Geochem Geophy Geosy,* n/a–n/a, **11**. 10.1029/2010gc003071.

Paterson, G.A., Tauxe, L. & Biggin, A.J., 2014. On improving the selection of paleointensity data. *Geochem. Geophys. Geosyst.,* **15,** 1180–1192. 10.1002/2013GC005135.

Pidgeon, R.T. & Wilde, S.A., 1990. The distribution of 3.0 Ga and 2.7 Ga volcanic episodes in the Yilgarn Craton of Western Australia. *Precambrian Res.,* **48,** 309–325. 10.1016/0301-9268(90)90015-I.

Poletti, W., Hartmann, G.A., Hill, M.J., Biggin, A.J. & Trindade, R.I.F., 2013. The cooling-rate effect on microwave archeointensity estimates. *Geophys. Res. Lett.,* **40,** 3847–3852. 10.1002/grl.50762.

Rolph, T.C. & Shaw, J., 1985. A new method of paleofield magnitude correction for thermally altered samples and its application to Lower Carboniferous lavas. *Geophys. J. R. astr. Soc.,* **80,** 773–781. 10.1111/j.1365-246X.1985.tb05124.x.

Selkin, P.A., Gee, J.S., Meurer, W.P. & Hemming, S.R., 2008. Paleointensity record from the 2.7 Ga Stillwater Complex, Montana. *Geochem. Geophys. Geosyst.,* **9**. 10.1029/2008GC001950.

Selkin, P.A., Gee, J.S. & Tauxe, L., 2007. Nonlinear thermoremanence acquisition and implications for paleointensity data. *Earth planet. Sci. Lett.,* **256,** 81–89. 10.1016/j.epsl.2007.01.017.

Shaw, J., 1974. A new method of determining the magnitude of the palaeomagnetic field, application to five historic lavas and five archaeological samples., *Geophys. J. R. astr. Soc.,* **39,** 133–141. 10.1111/j.1365-246X.1974.tb05443.x.

Shcherbakov, V.P., Gribov, S.K., Lhuillier, F., Aphinogenova, N.A. & Tsel'movich, V.A., 2019. On the reliability of absolute palaeointensity determinations on basaltic rocks bearing a thermochemical remanence. *J. geophys. Res.—Solid Earth,* **124,** 7616–7632. 10.1029/2019JB017873.

Shcherbakova, V.V., Bakhmutov, V.G., Thallner, D., Shcherbakov, V.P., Zhidkov, G.V. & Biggin, A.J., 2019. Ultra-low palaeointensities from East European Craton, Ukraine support a globally anomalous palaeomagnetic field in the Ediacaran. *Geophys. J. Int.,* **220,** 1928–1946.

Shcherbakova, V.V., Lubnina, N.V., Shcherbakov, V.P., Zhidkov, G.V. & Tsel'movich, V.A., 2017. Paleointensity determination on Neoarchaean dikes within the Vodlozerskii terrane of the Karelian craton. *Izv. Phys. Solid Earth,* **53,** 714–732. 10.1134/S1069351317050111.

Smirnov, A.V. & Evans, D.A.D., 2015. Geomagnetic paleointensity at ~2.41 Ga as recorded by the Widgiemooltha Dike Swarm, Western Australia. *Earth planet. Sci. Lett.,* **416,** 35–45.

Smirnov, A.V., Evans, D.A.D., Ernst, R.E., Söderlund, U. & Li, Z.-X., 2013. Trading partners: tectonic ancestry of southern Africa and western Australia, in Archean supercratons Vaalbara and Zimgarn. *Precambrian Res.,* **224,** 11–22. 10.1016/j.precamres.2012.09.020.

Smirnov, A.V., Kulakov, E.V., Foucher, M.S. & Bristol, K.E., 2017. Intrinsic paleointensity bias and the long-term history of the geodynamo. *Sci. Adv.,* **3,** e1602306. 10.1126/sciadv.1602306.

Smirnov, A.V. & Tarduno, J.A., 2005. Thermochemical remanent magnetization in Precambrian rocks: are we sure the geomagnetic field was weak?, *J. geophys. Res.—Solid Earth,* **110,** B06103. 10.1126/sciadv.1602306.

Smirnov, A.V., Tarduno, J.A. & Evans, D.A.D., 2011. Evolving core conditions ca. 2 billion years ago detected by paleosecular variation. *Phys Earth planet. Inter.,* **187,** 225–231. 10.1016/j.pepi.2011.05.003.

Smirnov, A.V., Tarduno, J.A., Kulakov, E.V., McEnroe, S.A. & Bono, R.K., 2016. Palaeointensity, core thermal conductivity and the unknown age of the inner core. *Geophys. J. Int.,* **205,** 1190–1195. 10.1093/gji/ggw080.

Smirnov, A.V., Tarduno, J.A. & Pisakin, B.N., 2003. Paleointensity of the early geodynamo (2.45 Ga) as recorded in Karelia: a single-crystal approach. *Geology,* **31,** 415–418. 10.1130/0091-7613(2003)0312.0.CO;2.

Smithies, R.H. & Champion, D.C., 1999. Late Archaean felsic alkaline igneous rocks in the Eastern Goldfields, Yilgarn Craton, Western Australia: a result of lower crustal delamination?, *J. Geol. Soc. London,* **156,** 561–576. 10.1144/gsjgs.156.3.0561.

Sprain, C.J., Swanson-Hysell, N.L., Fairchild, L.M. & Gaastra, K., 2018. A field like today's? The strength of the geomagnetic field 1.1 billion years ago. *Geophys. J. Int.,* **213,** 1969–1983. 10.1093/gji/ggy074.

Stark, J.C., Wilde, S.A., Söderlund, U., Li, Z.-X., Rasmussen, B. & Zi, J.-W., 2018. First evidence of Archean mafic dykes at 2.62 Ga in the Yilgarn Craton, Western Australia: links to cratonisation and the Zimbabwe Craton. *Precambrian Res.,* **317,** 1–13. 10.1016/j.precamres.2018.08.004.

Suttie, N., Shaw, J. & Hill, M.J., 2010. Direct demonstration of microwave demagnetization of a whole rock sample with minimal heating. *Earth planet. Sci. Lett.,* **292,** 357–362. 10.1016/j.epsl.2010.02.002.

Tauxe, L. & Staudigel, H., 2004. Strength of the geomagnetic field in the Cretaceous Normal Superchron: new data from submarine basaltic glass of the Troodos Ophiolite. *Geochem. Geophys. Geosyst.,* **5,** art. no. Q02H06. 10.1029/2003GC000635.

Thallner, D., Biggin, A.J. & Halls, H.C., 2021a. An extended period of extremely weak geomagnetic field suggested by palaeointensities from the Ediacaran Grenville dykes (SE Canada). *Earth planet. Sci. Lett.,* **568,** 117025. 10.1016/j.epsl.2021.117025.

Thallner, D., Biggin, A.J., McCausland, P.J.A. & Fu, R.R., 2021b. New paleointensities from the skinner cove formation, newfoundland, suggest a changing State of the geomagnetic field at the Ediacaran-Cambrian transition. *J. geophys. Res.—Solid Earth,* **126,** e2021JB022292. 10.1029/2021JB022292.

Thallner, D., Shcherbakova, V.V., Bakhmutov, V.G., Shcherbakov, V.P., Zhidkov, G.V., Poliachenko, I.B. & Biggin, A.J., 2022. New palaeodirections and palaeointensity data from extensive profiles through the Ediacaran section of the Volyn Basalt Province (NW Ukraine). *Geophys. J. Int.,* **231,** 474–492. 10.1093/gji/ggac186.

Tsunakawa, H. & Shaw, J., 1994. The shaw method of palaeointensity determinations and its application to recent volcanic-rocks. *Geophys. J. Int.,* **118,** 781–787. 10.1111/j.1365-246X.1994.tb03999.x.

Valet, J.P., Besse, J., Kumar, A., Vadakke-Chanat, S. & Philippe, E., 2014. The intensity of the geomagnetic field from 2.4 Ga old Indian dykes. *Geochem. Geophys. Geosyst.,* **15,** 2426–2437. 10.1002/2014GC005296.

Veikkolainen, T. & Pesonen, L.J., 2014. Palaeosecular variation, field reversals and the stability of the geodynamo in the Precambrian. *Geophys. J. Int.,* **199,** 1515–1526. 10.1093/gji/ggu348.

Verwey, E. J. W., 1939. Electronic Conduction of Magnetite (Fe3O4) and its Transition Point at Low Temperatures, *Nature,* **144**(), 327–328. 10.1038/144327b0.

Wilde, S.A. & Pidgeon, R.T., 1987. Geochronology, geothermometry and petrology of the main areas of gold mineralization in the Wheat Belt Region of Western Australia. *Western Australian Mining and Petroleum Research Institute,* Project 30. https://www.mriwa.wa.gov.au/research-projects/project-portfolio/u-pb-geochronology-geothermometry-and-petrology-of-the-main-areas-of-gold-mineralisation-in-the-wheat-belt-region-of-w-a/.

Yamamoto, Y., Tsunakawa, H. & Shibuya, H., 2003. Palaeointensity study of the Hawaiian 1960 lava: implications for possible causes of erroneously high intensities. *Geophys. J. Int.,* **153,** 263–276. 10.1046/j.1365-246X.2003.01909.x.

Yoshihara, A. & Hamano, Y., 2000. Intensity of the Earth's magnetic field in late Archean obtained from diabase dikes of the Slave Province, Canada. *Phys. Earth planet. Inter.,* **117,** 295–307. 10.1016/S0031-9201(99)00103-X.

Yu, Y.J. & Tauxe, L., 2005. Testing the IZZI protocol of geomagnetic field intensity determination. *Geochem Geophy Geosy,* **6**. 10.1029/2004GC000840.

Zhang, Y., Swanson-Hysell, N.L., Avery, M.S. & Fu, R.R., 2022. High geomagnetic field intensity recorded by anorthosite xenoliths requires a strongly powered late Mesoproterozoic geodynamo. *Proc. Natl. Acad. Sci.,* **119,** e2202875119. 10.1073/pnas.2202875119.

Zhou, T. *et al.* 2022. Early Cambrian renewal of the geodynamo and the origin of inner core structure. *Nat. Commun.,* **13,** 4161. 10.1038/s41467-022-31677-7.